A Comparison of Low-Frequency Noise Characteristics and Noise Sources in NPN and PNP InP-Based Heterojunction Bipolar Transistors

Shawn S. H. Hsu and Dimitris Pavlidis, *Fellow, IEEE*

***Abstract*—Low-frequency noise characteristics of NPN and PNP InP-based heterojunction bipolar transistors (HBTs) were investigated. NPN HBTs showed a lower base noise current level (3.85 $\times$ 10^{-17} A^2/Hz) than PNP HBTs (3.10 $\times$ 10^{-16} A^2/Hz), but higher collector noise current level (7.16 $\times$ 10^{-16} A^2/Hz) than PNP HBTs (1.48 $\times$ 10^{-16} A^2/Hz) at 10 Hz under $I_C = 1$ mA, $V_C = 1$ V. The NPN devices showed a weak dependence $I_C^{0.77}$ of the collector noise current, and a dependence $I_B^{1.18}$ of the base noise current, while the PNP devices showed dependences $I_C^{1.92}$ and $I_B^{1.54}$, respectively. The dominant noise sources and relative intrinsic noise strength were found in both NPN and PNP InP-based HBTs by comparing the noise spectral density with and without the emitter feedback resistor. Equivalent circuit models were employed and intrinsic noise sources were extracted. The high base noise current of PNP HBTs could be attributed to the exposed emitter periphery and higher electron surface recombination velocity in P-type InP materials, while the relatively high collector noise current of NPN HBTs may be due to the noise source originating from generation-recombination process in the bulk material between the emitter and the collector.**

***Index Terms*—Heterojunction bipolar transistors, noise.**

I. Introduction

LOW-FREQUENCY noise characteristics have been investigated for both bipolar junction transistors (BJTs) and heterojunction bipolar transistors (HBTs) [1]–[4]. The diffusion process in the bulk material and the recombination process in the base surface have been reported as sources of $1/f$ noise [1], [2]. The traps existing in devices have also been identified as sources of generation-recombination (G-R) noise [3]. The diffusion noise due to mobility fluctuation represents a fundamental limit to $1/f$ noise. On the other hand, the recombination noise reflects the impact of material and technology used for devices and can be related to device reliability [5].

The low-frequency noise characteristics of HBTs have been reported for different material systems. Tutt *et al.* [3] reported that the low-frequency noise of AlGaAs/GaAs power HBTs was limited by technology rather than the fundamental diffusion noise mechanism. D. Costa *et al.* [2] concluded that fluctuations in the extrinsic-base surface recombination velocity are the origin of the $1/f$ noise in small-geometry AlGaAs/GaAs HBTs. Kleinpenning *et al.* [6] investigated the impact of parasitic resistances on the $1/f$ noise characteristics in n-p-n AlGaAs/GaAs HBTs, and concluded that the noise contributed from parasitic series resistances becomes important at high forward current.

In InP-based HBTs, only little has been reported for the low-frequency noise characteristics of NPN HBTs, and no reports exist for PNP HBTs, except a recent paper published by the authors [29]. Tanaka *et al.* [7] reported that the base noise current spectra of InAlAs/InGaAs HBTs were found to be 20 dB lower than those of AlGaAs/GaAs HBTs under the same bias conditions. They also found that $S_{Ib}(f)$ is proportional to $I_b^{1.7}$, and concluded that the base noise current is surface recombination limited. Y. Takanaishi *et al.* [8] measured low-frequency noise in InP/InGaAs HBTs with different periphery/area (P/A) ratios and concluded that the main low-frequency noise is recombination of electrons at the exposed base surface near the emitter edge. J. Cowles *et al.* [9] observed a weak dependence of 0.54 for the collector noise on the collector current in InAlAs/InGaAs NPN HBTs. In addition, $S_{Ic}(f)$ was independent of the P/A ratio and the origin of the low-frequency noise was suggested to be from bulk rather than recombination process in the exposed base area. Borgarino *et al.* [10] reported InP/InGaAs HBTs with a base ideality factor of 1.02, and a $1/f$ noise figure-of-merit of $\sim 2 \times 10^{-8}$ μm^2. They suggested that the surface recombination from the extrinsic base region is not the dominant base low-frequency noise source.

Based on the above, it appears that different conclusions have been drawn from the observed low-frequency noise characteristics of InP-based HBTs and further studies could therefore be useful. Due to low surface recombination velocity of InP-based materials, one may expect that the low-frequency noise of the InP-based HBTs is limited by the fundamental diffusion noise mechanism. However, surface recombination is a noisy process, it may still dominate the noise performance of the devices. Moreover, the reported results of terminal noise dependence on bias current may not lead to a concrete conclusion. Deviations between the internal noise sources and measured terminal noise characteristics may exist due to device parasitic resistances [11]. In addition, as explained later, the external noise observed from one terminal can be generated from different internal noise sources.

In this paper, the low-frequency noise characteristics of both NPN and PNP InP-based HBTs were studied. Section II describes the layer structure, device characteristics and the noise measurement setup. Section III discusses various noise models

Manuscript received February 1, 2003; revised May 7, 2003. This work was supported by ARO (MURI Contract DAAHO4-96-1-0001) and NTT Photonics Laboratories. The review of this paper was arranged by Editor J. Deen.

The authors are with the Department of Electrical Engineering and Computer Science, University of Michigan, Ann Arbor, MI 48109-2122 USA.

Digital Object Identifier 10.1109/TED.2003.815367

0018-9383/03$17.00 © 2003 IEEE

TABLE I
EPITAXIAL LAYER STRUCTURES OF InP-BASED NPN AND PNP HBTs

Layer	Material	Thickness (Å)	Type	Doping (cm^{-3})
	NPN/PNP	NPN/PNP	NPN/PNP	NPN/PNP
Emitter cap	InGaAs/InGaAs	2000/2000	N^+/P^+	$2\times10^{19}/2\times10^{19}$
	InP/InAlAs	700/700	N^+/P^+	$2\times10^{19}/1\times10^{19}$
Emitter	InP/InAlAs	1500/1500	N/P	$5\times10^{17}/8\times10^{17}$
Spacer	InGaAs/InGaAs	100/100	I	---
Base	InGaAs/InGaAs	600/500	P^+/N^+	$1.5\times10^{19}/5\times10^{18}$
Collector	InGaAs/InGaAs	5000/3000	N^-/P^-	$5\times10^{16}/3\times10^{16}$
Subcollector	InGaAs/InGaAs	5000/5000	N^+/P^+	$2\times10^{19}/1\times10^{19}$
Buffer	InP/ (InGaAs/InAlAs supperlattice)	2000/1000	I	---
Substrate	InP		Semi-insulating	

used in this study. The physical origins of noise sources and the impact of emitter feedback resistor on the device terminal noise are considered. Section IV presents the noise measurement results for both NPN and PNP HBTs. The internal noise sources are calculated and the dependence of low-frequency noise on biasing current is also discussed. Section V concludes this work.

II. DEVICE CHARACTERISTICS AND MEASUREMENT SETUP

The InP/InGaAs NPN and InAlAs/InGaAs PNP HBTs in this study were both grown on InP substrates and their layer structures are shown in Table I. Both devices have similar structure except that the NPN HBTs had an InP emitter, while the PNP devices used InAlAs as the emitter. In addition, the PNP HBTs had slightly thinner and lower doped base than the NPN HBTs. The devices were both fabricated using the in-house developed self-aligned HBT process, which has a 0.2-μm base contact-to-emitter separation. Both device types demonstrated good microwave characteristics. Their use in complementary microwave circuits was reported in [12]. The 5×10 μm^2 NPN HBTs showed $f_T = 97$ GHz, and $f_{\max} = 51$ GHz at $I_C = 46$ mA, $V_{CE} = 2.0$ V, while the 5×10 μm^2 PNP HBTs showed $f_T = 11$ GHz, and $f_{\max} = 31$ GHz at $I_C = 11.7$ mA, $V_{EC} = 4.0$ V, which is the best InP-based PNP HBTs performance reported to date. The NPNs selected in this study match well the PNP HBTs in terms of technology and performance, and provide therefore a good reference for comparison.

Fig. 1 shows the forward Gummel plots for 5×10 μm^2 NPN and PNP HBTs. The NPN devices showed smaller base current than the PNP devices under the same collector current level. Assuming that recombination dominates the base current characteristics, which is normally the case in HBTs, the NPN devices appear to have smaller recombination current than the PNP HBTs. The ideality factors are 1.10 and 1.34 for $n(I_C)$ and $n(I_B)$ for the NPNs and the corresponding values for the PNPs are 1.09 and 1.9. The collector current ideality factors of both devices are similar and close to unity. The high base ideality factors in particular for PNP HBTs indicate a significant E–B region recombination process, which could result in higher low-frequency base noise.

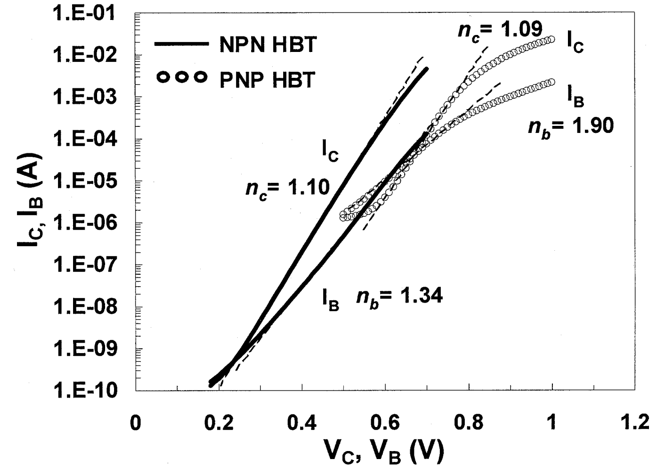

Fig. 1. Forward Gummel plots for 5×10 μm^2 NPN and PNP InP-based HBTs. The ideality factors are n_c and n_b for I_C and I_B, respectively.

Low-frequency noise was measured on both base noise current spectral density (collector short-circuited) and collector noise current spectral density (base short-circuited). The measured base and collector noise current spectral densities are denoted as $S_{Ib}(f)$ and $S_{Ic}(f)$, respectively. Batteries were used as power supplies to minimize the noise generated from biasing sources. Large capacitors ($\sim$mF) were used to provide AC ground and further reduce undesired noises from biasing sources. A bias resistor ($\sim$kΩ) was used at the input to provide a constant base current biasing. A low-noise amplifier (LNA) with a 60 dB voltage gain, and a high dynamic range spectrum analyzer (HP3561A) were employed to obtain the noise data. Load resistors (R_L) were inserted between the device and LNA to provide a low impedance path for the noise current. The noise current was converted to noise voltage through R_L, and then amplified by the LNA. Small wirewound resistors (typically 50$\sim$200 Ω) were used for R_L to minimize their

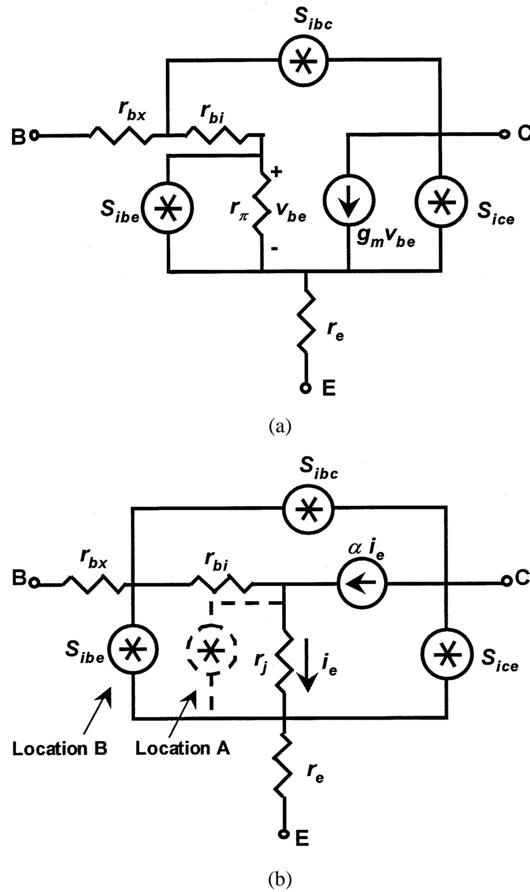

Fig. 2. Equivalent circuit models for BJTs and HBTs including three independent noise sources: (a) Pi-model and (b) Tee-model.

thermal and $1/f$ noise contribution. The measurements were performed from 10 Hz to 100 kHz. Averages of 50∼100 measurements were taken for lower frequency decades, and 200∼300 measurements were taken for higher frequency decades. The measured noise levels were well above the noise floor of the system.

III. Low-Frequency Noise Models

A. *Analysis of Various Noise Models*

Van der Ziel *et al.* [4] proposed a low-frequency noise equivalent circuit model for BJTs and HBTs, which used a Pi configuration. This model was applied to explain the low-frequency noise characteristics of BJTs [1], [13]. Tutt *et al.* [3] proposed a model based on the previous one, but used a Tee configuration. Both models are shown in Fig. 2(a) and (b). The models include three noise current sources:

1) S_{ibe};
2) S_{ibc};
3) S_{ice}.

Note that S_{ibe} is placed in two different positions in Fig. 2(b). The significance of each choice will be discussed later. The noise source S_{ibe} represents the noise originated in the base-emitter region. In BJTs, S_{ibe} is mainly attributed to the diffusion $1/f$ mechanism. However, in HBTs, due to their exposed emitter-base area and heterojunction, the recombination noise plays an important role. S_{ice} is connected between the emitter and the collector to describe the noise current flowing directly between these two terminals. Ideally, S_{ice} is the $1/f$ noise generated from the carrier diffusion process in BJTs. The $1/f$ noise due to the generation-recombination process is another possible source contributing to S_{ice} in HBTs. S_{ibc} is connected between the base and the collector and is associated with the surface recombination $1/f$ noise mechanism. It may also be correlated with partition noise since injected carriers either flow to the base or to the collector [4]. The magnitude of S_{ibc} is usually relatively small since the B–C junction is reverse-biased under the forward active condition. The Pi- and the Tee-model can be converted mutually by well-known equations. Although the Tee-model is a better physical representation than the Pi-model at high frequencies [14], they are basically identical at low frequencies. By converting van der Ziel's model, one can obtain the Tee-model in Fig. 2(b) with S_{ibe} in position A. However, Tutt *et al.* [3] proposed that S_{ibe} may flow through part of the base resistance in HBTs, and therefore it is more appropriate to have it connected in position B. $S_{Ib}(f)$ and $S_{Ic}(f)$ can be obtained based on the Tee-model with S_{ibe} connected in position A (assuming S_{ibc} is negligible)

$$\begin{aligned} S_{Ib}(f) &= S_{ibe}\left[\frac{r_j + r_e\alpha}{r_j + r_e + r_b(1-\alpha)}\right]^2 \\ &\quad + S_{ice}\left[\frac{r_e(1-\alpha)}{r_j + r_e + r_b(1-\alpha)}\right]^2 \end{aligned} \tag{1}$$

$$\begin{aligned} S_{Ic}(f) &= S_{ibe}\left[\frac{r_e\alpha}{r_j + r_e + r_b(1-\alpha)}\right]^2 \\ &\quad + S_{ice}\left[\frac{r_j + (r_e + r_b)(1-\alpha)}{r_j + r_e + r_b(1-\alpha)}\right]^2. \end{aligned} \tag{2}$$

On the other hand, if the calculation is based on the connection of S_{ibe} in position B, then the following equations hold:

$$\begin{aligned} S_{Ib}(f) &= S_{ibe}\left[\frac{r_j + r_e\alpha + r_{bi}(1-\alpha)}{r_j + r_e + r_b(1-\alpha)}\right]^2 \\ &\quad + S_{ice}\left[\frac{r_e(1-\alpha)}{r_j + r_e + r_b(1-\alpha)}\right]^2 \end{aligned} \tag{3}$$

$$\begin{aligned} S_{Ic}(f) &= S_{ibe}\left[\frac{\alpha(r_e + r_{bx})}{r_j + r_e + r_b(1-\alpha)}\right]^2 \\ &\quad + S_{ice}\left[\frac{r_j + (r_e + r_b)(1-\alpha)}{r_j + r_e + r_b(1-\alpha)}\right]^2. \end{aligned} \tag{4}$$

By comparing (1) and (3), one finds, as expected that only the S_{ibe}-related terms are different. Moreover, the difference between the two equations may not be negligible when r_e and α are small and r_{bi} is relatively large. From (2) and (4), the difference is more obvious, since r_{bx} could be similar or even larger than r_e. As can be seen, these two models can give different results, and a better physical representation of the noise mechanism is necessary, as attempted for the devices studied in this work. As mentioned above, the base recombination current could be significant, and the conducting path of the recombination current is unlikely to flow completely inside the base region. The model proposed by Tutt *et al.* is therefore more appropriate to be used in this work.

The low-frequency noise model of BJTs and HBTs proposed by Kleinpenning neglects S_{ibc} and includes $1/f$ and thermal noise from parasitic resistances [15]. The base and collector terminal noises based on the model of [15] are also similar to (1) to (4), if one uses $r_b = r_{bx}$ and $r_{bi} = 0$, which hold when S_{ibe} is connected outside the base resistance. One additional term in his noise model equation of [15] is related to $1/f$ and thermal noise from the base and emitter resistances. This model will be used to explain some of the observed noise dependence on biasing current in Section IV.

B. Impact of Emitter Feedback on Terminal Noise Current Characteristics

The emitter feedback resistor (R_E) technique was employed to help analyzing the intrinsic noise source characteristics. As R_E is inserted between the emitter and ground, one can simply rewrite the equations by replacing r_e with $(r_e + R_E)$. The impact of R_E on terminal noise characteristics can then be investigated using (3) and (4). Assuming that the original coefficient of each intrinsic noise source is $(A/B)^2$ in any of these equations, then the coefficient becomes $[(A + \Delta A)/(B + \Delta B)]^2$ when R_E is added. If $\Delta A/\Delta B > A/B$, the coefficient becomes larger, while if $\Delta A/\Delta B < A/B$, the opposite hold. For example, the coefficient of S_{ibe} in (3) decreases when R_E is inserted, since A/B in this case is very close to one, while $\Delta A/\Delta B$ equals α (the transport factor of the device), which is smaller than one. As a result, the contribution of S_{ibe} to $S_{Ib}(f)$ reduces when R_E is inserted. On the other hand, the coefficient of S_{ibe} in (4) increases with emitter feedback since $\Delta A/\Delta B > A/B$ in this case. Similarly, as a result of adding R_E, S_{ice}'s contribution to $S_{Ib}(f)$ increases, while its contribution to $S_{Ic}(f)$ decreases dramatically. Details of the above trends will be shown using the actual parameters of the tested devices in Section IV.

IV. Measurement Results and Discussion

A. Low-Frequency Noise Characteristics for NPN and PNP InP HBTs

Fig. 3 shows $S_{Ib}(f)$ and $S_{Ic}(f)$ for both 5×10 μm^2 NPN and PNP HBTs under the same collector current and voltage ($I_C = 1$ mA, $V_C = 1$ V). The NPN device shows a significantly higher $S_{Ic}(f)$ than $S_{Ib}(f)$, while the PNP device shows a higher $S_{Ib}(f)$ than $S_{Ic}(f)$. Assuming that S_{ibe} and S_{ice} are the two dominant noise sources in these HBTs, the measured results suggest that S_{ice} (NPN) is significantly higher than S_{ibe} (NPN) under this current level. On the other hand, S_{ice} (PNP) is lower than S_{ibe} (PNP). In addition, both S_{ice} (PNP) and S_{ibe} (PNP) are smaller than S_{ice} (NPN), but larger than S_{ibe} (NPN). Note that this conclusion is based on the assumption that $S_{Ib}(f) \sim S_{ibe}$ and $S_{Ic}(f) \sim S_{ice}$, which allows one to make an approximate comparison of the relative intrinsic noise levels. For detailed information of intrinsic noise sources, one needs to use actual device parameters to calculate the contribution of intrinsic noise sources to the terminal noise characteristics.

Based on Gummel plot results, a higher base noise level is expected from PNPs since they present significantly higher base recombination current than the NPNs. The higher collector noise level of NPNs than PNPs could be possibly attributed to the G-R $1/f$ noise originated in the conducting path and the bulk material of NPN devices due to traps and interface states. In addition, a smaller exponent γ of the $1/f^\gamma$ characteristic was observed for NPNs ($\gamma \sim 0.8$) than PNPs ($\gamma \sim 1.0$) for both $S_{Ib}(f)$ and $S_{Ic}(f)$. Mohammadi *et al.* [5] reported that for high-reliability HBTs, γ decreased from 1.01 to 0.7 after high current and high temperature stress due to the increase of G-R noise with respect to the $1/f$ component. Since a wide distribution of G-R time constants can produce a $1/f^\gamma$ spectrum, where γ can be smaller than one, the observed smaller $1/f$ roll-off of the NPN devices may be due to their higher G-R noise components in the bulk material than in the PNP devices. This explanation is consistent with the observed high $S_{Ic}(f)$ of the NPNs.

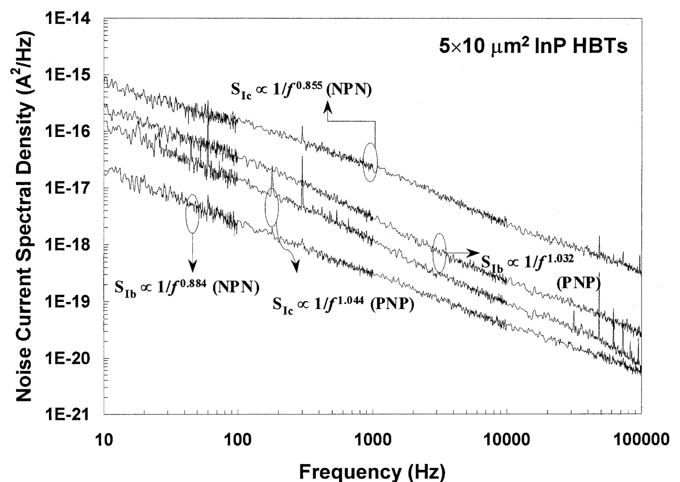

Fig. 3. Low-frequency base and collector noise characteristics of 5×10 μm^2 NPN and PNP InP-based HBTs. S_{Ic}(NPN) $\gg$ S_{Ib}(NPN), while S_{Ic}(PNP) $<$ S_{Ib}(PNP) under this bias condition. $I_B = 0.0743$ mA and 0.21 mA for NPN and PNP; $I_C = 1$ mA and $V_C = 1$ V for both devices.

B. Analysis and Comparison of Intrinsic Noise Sources

Fig. 4(a) and (b) show $S_{Ib}(f)$, $S'_{Ib}(f)$, $S_{Ic}(f)$, and $S'_{Ic}(f)$ of 5×10 μm^2 NPN HBTs under both low ($I_B = 0.0451$ mA, $I_C = 0.5$ mA, $V_{CE} = 1$ V) and high ($I_B = 0.338$ mA, $I_C = 10$ mA, $V_{CE} = 2$ V) bias conditions, where $S'_{Ib}(f)$ and $S'_{Ic}(f)$ are measured with the emitter feedback resistor. In Fig. 4(a), $S'_{Ib}(f)$ is lower than $S_{Ib}(f)$, while $S'_{Ic}(f)$ is significantly lower than $S_{Ic}(f)$. Based on Section IV-B, the results indicate that S_{ibe} and S_{ice} dominate the base and the collector terminal noise characteristics, respectively. The slightly higher $S'_{Ib}(f)$ than $S_{Ib}(f)$ in Fig. 4(b) indicates that S_{ice} is relatively large comparing to S_{ibe}. As R_E is inserted, the reverse isolation from collector to base reduces and the impact of S_{ice} on the base noise increases. If S_{ice} is large, it can impact the base terminal noise. Compared to the results in [1] for Si BJTs, where $S'_{Ic}(f)$ was found to be very close to $S_{Ic}(f)$ and $S_{Ib}(f)$ and S_{ice} was much smaller than S_{ibe}, the results obtained here show that both S_{ibe} and S_{ice} are important in determining the terminal noise characteristics.

Fig. 5 shows the results of PNPs. In Fig. 5(a), $S'_{Ib}(f)$ is slightly smaller than $S_{Ib}(f)$, which can be explained similar to Fig. 4(a). On the other hand, the larger $S'_{Ic}(f)$ than $S_{Ic}(f)$ reflects the fact that S_{ibe} is relatively large in PNPs. The

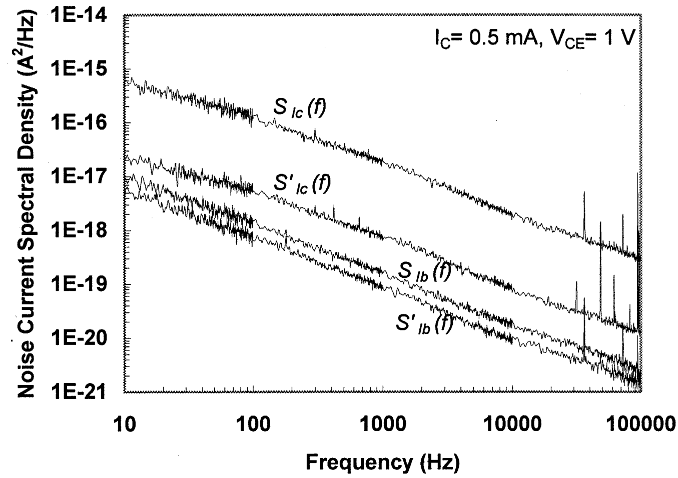

(a)

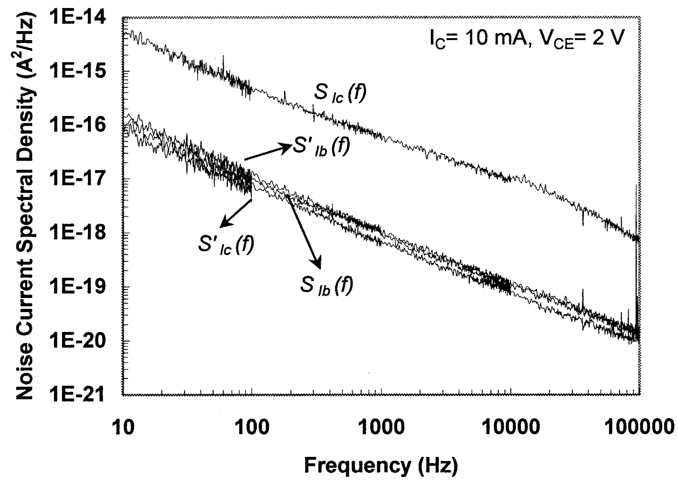

(b)

Fig. 4. Base and collector noise current spectral densities for 5 × 10 μm^2 NPN devices without and with the emitter feedback resistor: (a) at low bias level, $I_C = 0.5$ mA, $I_B = 0.0451$ mA, $V_{CE} = 1$ V and (b) at high bias level, $I_C = 10$ mA, $I_B = 0.338$ mA, $V_{CE} = 2$ V.

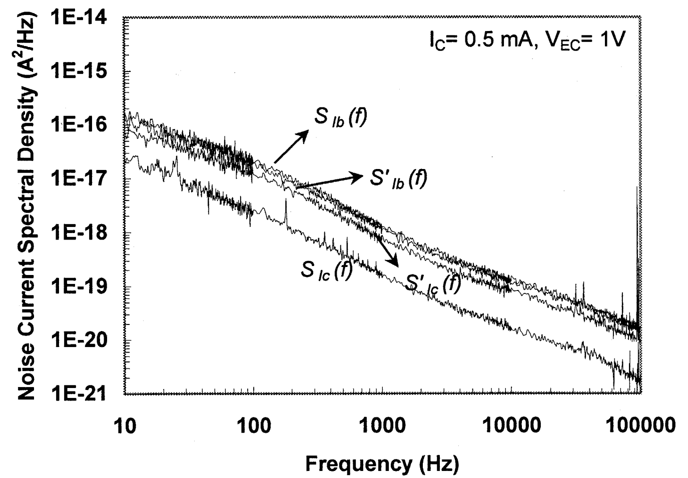

(a)

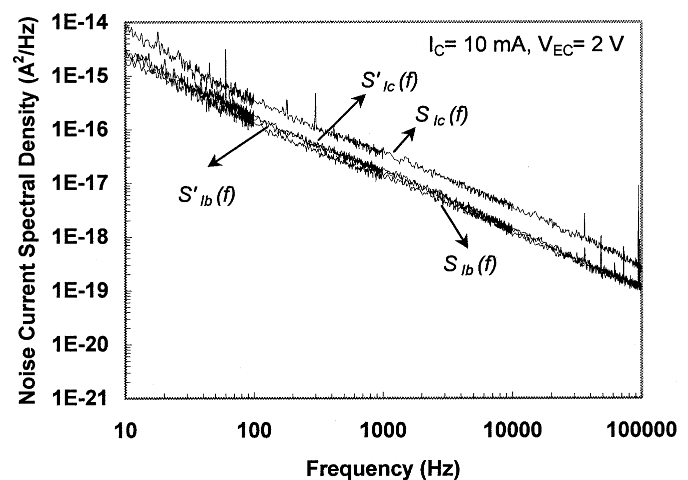

(b)

Fig. 5. Base and collector noise current spectral densities for 5 × 10 μm^2 PNP devices without and with emitter feedback resistor: (a) at low bias level, $I_C = 0.5$ mA, $I_B = 0.143$ mA, $V_{EC} = 1$ V (b) at high bias level, $I_C = 10$ mA, $I_B = 0.687$ mA, $V_{EC} = 2$ V.

impact of S_{ibe} to the collector terminal noise increases as R_E is inserted. If S_{ibe} is small, for example in NPNs, one can only see significantly reduced $S_{Ic}(f)$. The result is consistent with our finding from the Gummel plots. In Fig. 5(b), one can see $S'_{Ib}(f) > S_{Ib}(f)$ and $S'_{Ic}(f) < S_{Ic}(f)$. The results indicate that the increase rate of S_{ice} is higher than S_{ibe} when the bias current increases and therefore at high current levels, S_{ice} becomes relatively large and show its impact on the base terminal after R_E is inserted.

C. Calculation of Noise Model Parameters

The device parameters needed in the noise model such as parasitic resistances were first extracted from S-parameters under the corresponding bias conditions [16]. The results provide information on the total base resistance but it is difficult to separate r_{bi} and r_{bx}. In addition, the internal and external base distributed resistances corresponding to the physical HBT structure may not represent the internal and external base resistances seen by the noise current. Therefore, optimization was performed under a fixed r_b value extracted from a certain bias condition to separate r_{bi} and r_{bx} by fitting the measured noise data. Note that there is no unique solution for r_{bi} and r_{bx}, but efforts were put to minimize the overall errors between measured and calculated terminal noise characteristics. The values of α were also adopted from ac extraction for consistency and therefore are different from the dc values.

The calculation was based on (3) and (4). From the equations, once the device parameters are obtained from S-parameters, one can solve S_{ibe} and S_{ice} using measured $S_{Ib}(f)$ and $S_{Ic}(f)$. $S'_{Ib}(f)$ and $S'_{Ic}(f)$ were also calculated from (3) and (4) with r_e replaced by $r_e + R_E$. The final values of S_{ibe} and S_{ice} were obtained by optimizing the calculated to the measured results for $S_{Ib}(f)$, $S_{Ic}(f)$, $S'_{Ib}(f)$ and $S'_{Ic}(f)$ simultaneously. The use of two additional conditions can reduce the uncertainty from the parameter extraction procedure.

Table II shows the extracted device parameters, intrinsic base (S_{ibe}) and collector (S_{ice}) noise sources, and terminal noises $S_{Ib}(f)$, $S_{Ic}(f)$, $S'_{Ib}(f)$,and $S'_{Ic}(f)$. Good agreement was obtained between calculated and measured results. From the extracted internal noise sources, at low current levels, the terminal noise values, $S_{Ib}(f)$ and $S_{Ic}(f)$, were found to be close to the internal noise sources, S_{ibe} and S_{ice} for both devices. In ad-

TABLE II
MEASURED AND CALCULATED NOISE MODEL PARAMETERS OF NPN AND PNP HBTs

Parameters and noise levels \ Devices and bias conditions	5×10 μm² NPN (I_B= 0.0451 mA, I_C= 0.5 mA)	5×10 μm² NPN (I_B= 0.338 mA, I_C= 10 mA)	5×10 μm² PNP (I_B= 0.143 mA, I_C= 0.5 mA)	5×10 μm² PNP (I_B= 0.687 mA, I_C= 10 mA)
r_e (ohm)	1.3	1.3	6.3	6.0
r_{bi} (ohm)	10.8	10.5	2.9	4.5
r_{bx} (ohm)	5.2	5.1	0.8	1.3
r_j (ohm)	25.2	2.8	74.1	3.6
α	0.974	0.981	0.885	0.903
S_{ibe} (A²/Hz) at 10 Hz	7.64 ×10⁻¹⁸	1.45 ×10⁻¹⁶	1.88 ×10⁻¹⁶	2.80 ×10⁻¹⁵
S_{ice} (A²/Hz) at 10 Hz	3.39 ×10⁻¹⁶	7.15 ×10⁻¹⁵	2.72 ×10⁻¹⁷	3.21 ×10⁻¹⁴
$S_{Ib}(10)$:measured (A²/Hz)	9.42×10⁻¹⁸	1.32 ×10⁻¹⁶	1.73 ×10⁻¹⁶	2.04 ×10⁻¹⁵
$S_{Ib}(10)$:calculated (A²/Hz)	7.55×10⁻¹⁸	1.37 ×10⁻¹⁶	1.84 ×10⁻¹⁶	2.51 ×10⁻¹⁵
$S_{Ic}(10)$:measured (A²/Hz)	4.92×10⁻¹⁶	4.39 ×10⁻¹⁵	2.46 ×10⁻¹⁷	7.87 ×10⁻¹⁵
$S_{Ic}(10)$:calculated (A²/Hz)	3.08×10⁻¹⁶	3.90 ×10⁻¹⁵	2.47 ×10⁻¹⁷	8.59 ×10⁻¹⁵
$S'_{Ib}(10)$:measured (A²/Hz)	4.27×10⁻¹⁸	1.46 ×10⁻¹⁶	1.71 ×10⁻¹⁶	3.81 ×10⁻¹⁵
$S'_{Ib}(10)$:calculated (A²/Hz)	7.45×10⁻¹⁸	1.42 ×10⁻¹⁶	1.60 ×10⁻¹⁶	2.61 ×10⁻¹⁵
$S'_{Ic}(10)$:measured (A²/Hz)	1.92×10⁻¹⁷	8.91 ×10⁻¹⁷	7.19 ×10⁻¹⁷	2.79 ×10⁻¹⁵
$S'_{Ic}(10)$:calculated (A²/Hz)	1.51×10⁻¹⁷	1.54 ×10⁻¹⁶	7.26 ×10⁻¹⁷	2.73 ×10⁻¹⁵

dition, $S_{Ib}(f)$ and S_{ibe} were also close even under high bias levels. However, deviation between S_{ice} and $S_{Ic}(f)$ was observed under high bias level for both devices. At low current level, the impact of base noise current on the collector terminal is small due to r_j is large and the forward gain is small. In addition, the impact of the collector noise current on the base terminal is negligible, since the base noise current level is relatively high and the reverse isolation between the collector and the base is also high. Under high bias conditions, $S_{Ib}(f)$ can still be represented by S_{ibe} since the reverse isolation from the collector to the base is still high, while only part of S_{ice} contribute to $S_{Ic}(f)$ since r_j is smaller and α is relatively larger. As a result, S_{ice} flows more toward the base and the emitter terminals instead of appearing at the collector node, and therefore $S_{Ic}(f) < S_{ice}$ was observed. Note that $S_{Ib}(f) \sim S_{ibe}$ can only be obtained by assuming that r_j is very large and the value of S_{ice} is not considerably larger than S_{ibe}. On the other hand, $S_{Ic}(f) \sim S_{ice}$ is only valid when r_j is large and S_{ibe} is not significantly larger than S_{ice}. To obtain accurate information about the intrinsic noise sources at high bias level, one needs to use corresponding device parameters and solve (3) and (4). This was for example done under the high bias condition shown in Table II. The results show that the noise current from measured $S_{Ic}(f)$ (4.39 $\times$ 10^{-15} A^2/Hz) is only ~61% of the accurate solution for the intrinsic noise current S_{ice} (7.15 $\times$ 10^{-15} A^2/Hz) for NPNs. In case of PNPs, the measured $S_{Ic}(f)$ (7.87 $\times$ 10^{-15} A^2/Hz) is only ~25% of the intrinsic S_{ice} (3.21 $\times$ 10^{-14} A^2/Hz).

D. Dependence of Noise on Bias Currents

The low-frequency noise characteristics of BJTs and HBTs manifest dependence on bias current due to the bias-dependent noise origins. Theoretical and experimental results have been reported on this subject [4], [17], [18]. From theoretical point of view, the noise current spectral density $S_I(f)$ is proportional to I if the diffusion process is the major mechanism for $1/f$ noise. On the other hand, for $1/f$ noise originating from carrier G-R processes in the surface, $S_I(f)$ is proportional to I^2. G. Blasquez *et al.* [19] proposed an alternative theory based on minority carriers trapping in the bulk of BJTs. This model leads to $S_I(f) \propto I$ even if the low-frequency noise originates from carrier trapping process. Mohammadi *et al.* [20] proposed a nonfundamental noise theory, in which the noise current dependence can vary significantly with the trap density and carrier lifetime probability distribution functions.

Experimental results were also reported. Zhang *et al.* [21] found that $S_{Ic}(f)$ shows a $I_C^{1.5}$ dependence in HBTs, and suggested that this noise is more likely due to a G-R $1/f$ noise source. Tutt *et al.* [3] found that $S_{Ib}(f)$ has a dependence close to two on I_B and interpreted the results as surface recombination noise. Kleinpenning [22] discussed this issue based on the impact of parasitic resistance, for example, a $S_{Ic}(f) \propto I_C^{0.5}$ dependence observed in Si BJTs was explained by the impact of the emitter series resistance. Takanashi *et al.* [8] investigated devices with different P/A ratio and proved that the observed $S_{Ib}(f) \propto I_B^{1.62-1.72}$ is due to I_B consists of different components.

Table III summarizes the observed dependence of the terminal noise characteristics and the extracted intrinsic noise sources on the biasing current. The noise levels were obtained at 10 Hz under various bias conditions. As can be seen, $S_{Ib}(f) \propto I_B^{1.18}$ and $S_{ibe} \propto I_B^{1.47}$ for NPNs were observed. The smaller dependence than the expected $S_I \propto I^2$ can be explained by the surface recombination current is only one

TABLE III
DEPENDENCE OF TERMINAL AND INTRINSIC NOISE CHARACTERISTICS ON BIASING CURRENT AT 10 Hz

	$S_{Ib} \propto I_B^n$	$S_{ibe} \propto I_B^n$	$S_{Ic} \propto I_C^n$	$S_{ice} \propto I_C^n$
NPN	n =1.18	n =1.47	n =0.77	n =1.02
PNP	n =1.54	n =1.68	n =1.92	n =2.36

component of the base current. Assuming that the ratio of the recombination current to the total base current reduces by 42% from low to high bias levels, the deviation from a $S_{ibe} \propto I_B^{2.0}$ trend can be explained. $S_{Ic}(f)$ for NPNs shows a relatively small dependence of 0.77 on I_C. A $S_{Ic}(f) \propto Ic^{0.54}$ has been reported by Cowles *et al.* [9] on InP-based HBTs and was explained by the slower variation of h_{fe} with I_C and lower nonideal surface recombination currents in InP HBTs. However, the relatively high collector noise level in the studied NPN HBTs implies that the noise is not limited by the fundamental diffusion noise mechanism but more likely the G-R processes, which has a theoretical prediction of $S_{Ic}(f) \propto I_C^2$. If one plots the intrinsic S_{ice} vs. I_C, where the impact of parasitic resistance on the external noise level through feedback is removed, the slope becomes 1.02. The weak dependence could be explained by the theory proposed by G. Blasquez, which is based on minority carriers trapping process in bulk. The model proposed by Mohammadi could also be applied to interpret the observed results, since a wide range of noise-current dependence is possible based on this theory.

For PNPs, it was found that $S_{Ib}(f) \propto I_B^{1.54}$ and $S_{ibe} \propto I_B^{1.68}$. This could also be attributed to the fact that surface recombination current is only part of the total base current. The dependence of $S_{Ib}(f)$ and S_{ibe} on I_B is closer to two in PNPs than NPNs and may be due to the recombination current contributing a larger portion of I_B in PNPs. On the other hand, $S_{Ic}(f) \propto I_C^{1.92}$ and $S_{ice} \propto I_C^{2.36}$ were observed. The high intrinsic noise dependence on the collector current can be explained by the $1/f$ noise generated from the parasitic resistances. Based on the equations in [15], if one neglects the contribution of S_{ibe}, and assumes $S_{ice} \propto I_C^2$, $r_\pi \gg \beta r_e$, $S_{Ic}(f)$ can be simplified to $\cong \mathrm{A} I_C^2 + \mathrm{B} I_C^4$. Since the model used for intrinsic noise source extraction did not include $1/f$ noise from parasitic resistances ($\mathrm{B} I_C^4$), one may overestimate S_{ice}. Therefore, a higher collector current dependence could be possible.

E. Comparison of Noise Characteristics in NPN and PNP HBTs

Fig. 6 shows the low-frequency noise of the NPN and PNP InP-based HBTs in this work, and also compares several results found in literature [8], [23], [24]. The results shown were obtained from a 5-μm diameter InP/InGaAs NPN HBT [8], a 21 μm^2 emitter InAlAs/InGaAs HBT [23], and a 22 μm^2 emitter self-aligned InP/InGaAs HBT [24]. As can be seen, the base noise levels of InP/InGaAs NPN HBTs in this study are comparable to [24] and slightly lower than [23] under similar base current levels. Compared to the results in [8], the noise levels reported here seem to be high under low base current levels, however, if one extrapolates the curve plotted from [8] up to I_B above ~200 μA, similar noise levels can be obtained. The

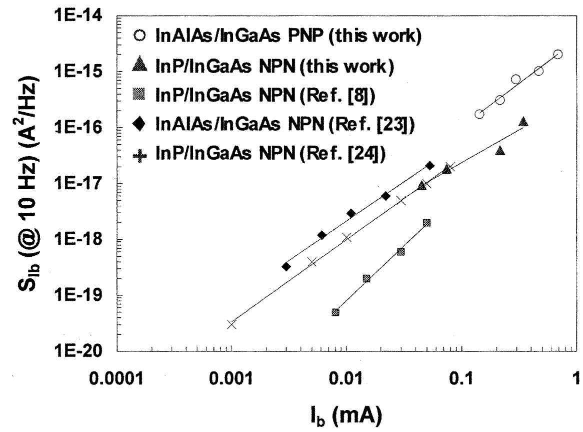

Fig. 6. Comparison of base noise characteristics for InP-based NPN and PNP HBTs. S_{Ib} is plotted as a function of I_B at 10 Hz.

NPN base current level used in this study is relatively high compared to other reports for a better match to the I_B of PNPs, since the PNP HBTs need to be biased under higher base current for proper device operation. In addition, the NPNs investigated had a relative smaller gain (~10 to 30) comparing to for example in [8] (~100 to 200) due to differences in device design. Therefore, a higher base current level was chosen so that the noise characteristics could be measured under bias used in circuit applications.

Compared to InP-based NPN HBTs, PNP HBTs present in general higher base noise levels even when similar base current levels were considered. The surface recombination velocity has been reported to be higher in P-type than that in N-type InP materials [25], [26]. The surface recombination velocity in semiconductor materials can be calculated by $v_{sn} \cong N_{rec} v_p \sigma_p n_0 / n_s$ and $v_{sp} \cong P_{rec} v_n \sigma_n p_0 / p_s$, where v_{sn} and v_{sp} are the surface recombination velocity for N and P materials; N_{rec} and P_{rec} are the area density of the surface recombination centers; v_p and v_n are unilateral mean velocities for electron and holes; σ_n and σ_p are the electron and hole capture cross-sections; n_0 and p_0 are doping concentrations; and n_s and p_s are the electron and hole concentrations at the surface [27]. Considering that the NPN, PNP devices had about the same base doping level, and they were processed in the same fashion, the n_0, p_0 and N_{rec}, P_{rec} are expected to be similar. Assuming equal capture cross sections for electrons and holes leads to speculate that the surface recombination velocity of holes in the N material is smaller than that of electrons in the P material used for base due to smaller v_p than v_n. Since the surface recombination current (I_R) is proportional to the surface recombination velocity (v_s), assuming $S_{IR}(f) \propto I_R^2$, a relation of $S_{IR}(f) \propto v_s^2$ can be obtained [28]. Based on the above and provided that base surface recombination is the major low-frequency noise mechanism, this could suggest that the noise level of NPN device is larger than PNP HBTs, which is contrary to our findings.

However, in addition to the recombination occurring close to the exposed base surface, carriers injected from the base to the emitter may also recombine at the emitter periphery/surface, which could be another major noise source in HBTs. For the HBTs investigated here, due to the use of a self-aligned base

process, the exposed base area is much smaller than the exposed emitter periphery area; the area ratio was calculated to be ∼1/3 for 5 × 10 μm^2 HBTs. It is therefore reasonable to assume that the surface recombination is dominated by the recombination current in the emitter periphery. Considering that surface recombination velocity for electrons in P-emitter of PNPs is higher than that of holes in N-emitter of NPNs, this can lead to a higher base recombination current and therefore higher base low-frequency noise in PNP HBTs. The result would be consistent with our findings of higher base noise levels for PNP than NPN devices. In addition to the analysis above, the noise dependence on different geometries is useful for identifying the noise origins if noise is mainly contributed from surface related problems. Studies along these lines have been investigated by the authors and recently published [29]. It was found that the device base noise shows a strong dependence on the P/A ratio. For example, comparing the PNP devices with P/A ratios of 0.87 (3 × 10 μm^2) and 2.07 (1 × 30 μm^2), a considerably higher base noise current was found for the devices with higher P/A ratio, which is a proof of surface-related noise sources. In addition, it also indicates that the device noise is not limited by the DX center in the InAlAs emitter for the PNP HBTs used in this study. The high base noise current level of PNP HBTs may be improved by proper passivation on the exposed emitter periphery, since the main low-frequency noise is generated from that area.

V. Conclusion

The low-frequency noise characteristics of InP-based NPN and PNP HBTs were investigated. Devices under different bias conditions were characterized. The emitter feedback technique was used to analyze the intrinsic noise sources and compare their relative levels. Different noise models were discussed. In addition, the measured terminal noise $S_{Ib}(f)$ and $S_{Ic}(f)$ can be used to approximate the intrinsic noise source S_{ibe} and S_{ice} at low current levels, while deviation were observed when the devices biased at high current levels for the collector noise. The observed noise current dependence for base can be explained by the base current is composed of different current components, the low dependence for S_{ice} on I_C in NPNs may be explained by minority carriers trapping process in bulk, and the high dependence for S_{ice} on I_C in PNPs may be explained by the impact of $1/f$ noise generated from parasitic resistances. Analysis of the intrinsic noise sources of NPN and PNP HBTs suggests that passivation on the exposed emitter periphery can improve the base noise current of NPN and PNP InP-based HBTs.

References

[1] A. Pawlikiewicz and A. van der Ziel, "Location of $1/f$ noise sources in BJTs and HBTs—II. Experiment," *IEEE Trans. Electron Devices*, vol. 34, pp. 2009–2012, Sept. 1987.

[2] D. Costa and J. S. Harris, "Low-frequency noise properties of n-p-n AlGaAs/GaAs heterojunction bipolar transistors," *IEEE Trans. Electron Devices*, vol. 39, pp. 2383–2394, Oct. 1992.

[3] M. Tutt, D. Pavlidis, A. Khatibzadeh, and B. Bayraktaroglu, "Low frequency noise characteristics of self-aligned AlGaAs/GaAs power heterojunction bipolar transistors," *IEEE Trans. Electron Devices*, vol. 43, pp. 219–230, Feb. 1995.

[4] A. van der Ziel, X. Zhang, and A. M. Pawlikiewicz, "Location of $1/f$ noise sources in BJTs and HBTs—I. Theory," *IEEE Trans. Electron Devices*, vol. 33, pp. 1371–1376, Sept. 1986.

[5] S. Mohammadi, D. Pavlidis, and B. Bayraktaroglu, "Relation between low-frequency noise and long-term reliability of single AlGaAs/GaAs power HBTs," *IEEE Trans. Electron Devices*, vol. 47, pp. 677–686, Apr. 2000.

[6] T. G. M. Kleinpenning and A. J. Holden, "$1/f$ noise in n-p-n GaAs/AlGaAs heterojunciton bipolar transistors: Impact of intrinsic transistor and parasitic series resistance," *IEEE Trans. Electron Devices*, vol. 40, pp. 1148–1153, June 1993.

[7] S. Tanaka, H. Hayama, A. Furukawa, T. Baba, M. Mizuta, and K. Honjo, "Low-frequency noise performance of self-aligned InAlAs/InGaAs heterojunction bipolar transistors," *Electron. Lett.*, vol. 26, pp. 1439–1441, 1990.

[8] Y. Takanashi and H. Fukano, "Low-frequency noise of InP/InGaAs heterojunction bipolar transistors," *IEEE Trans. Electron Devices*, vol. 45, pp. 2400–2406, Dec. 1998.

[9] J. Cowles, L. Tran, T. Block, D. Streit, C. Grossman, G. Chao, and A. Oki, "A comparison of low frequency noise in GaAs and InP-based HBTs and VCOs," in *Proc. IEEE MTT Symp.*, Orlando, FL, June 1995, pp. 689–692.

[10] M. Borgarino, R. Plana, M. Fendler, J. P. Vilcot, F. Mollot, J. Barette, D. Decoster, and J. Graffeuil, "Low frequency noise behavior of InP/InGaAs heterojunction bipolar waveguide phototransistors," *Solid-State Electron.*, vol. 44, pp. 59–62, Jan. 2000.

[11] T. G. M. Kleinpenning, "Low-frequency noise in modern bipolar transistors: Impact of intrinsic transistor and parasitic series resistances," *IEEE Trans. Electron Devices*, vol. 41, pp. 1981–1991, Nov. 1994.

[12] D. Sawdai and D. Pavlidis, "Push–pull circuits using n-p-n and p-n-p InP-based HBTs for power amplification," *IEEE Trans. Microwave Theory Tech.*, vol. 47, pp. 1439–1448, Aug. 1999.

[13] A. Pawlikiewicz, A. van der Ziel, G. S. Kousik, and C. M. van Vliet, "Fundamental $1/f$ noise in silicon bipolar transistors," *Solid-State Electron.*, vol. 31, no. 5, pp. 831–834, 1988.

[14] D. A. Teeter and W. R. Curtice, "Comparison of hybrid Pi and Tee HBT circuit topologies and their relationship to large signal modeling," in *Proc. IEEE MTT Symp.*, Denver, CO, June 1997, pp. 374–378.

[15] T. G. M. Kleinpenning, "Location of low-frequency noise sources in submicrometer bipolar transistors," *IEEE Trans. Electron Devices*, vol. 39, pp. 1501–1506, June 1992.

[16] D. Pehlke and D. Pavlidis, "Evaluation of the factors determining hbt high-frequency performance by direct analysis of s-parameter data," *IEEE Trans. Microwave Theory Tech.*, vol. 40, pp. 2367–2373, Dec. 1992.

[17] T. G. M. Kleinpenning, "$1/f$ noise in p-n diodes," *Physica*, vol. 98B, p. 289, 1980.

[18] F. N. Hooge, "$1/f$ noise is no surface effect," *Phys. Lett.*, vol. A-29, p. 139, 1969.

[19] G. Blasquez and D. Sauvage, "Flicker noise due to minority carriere trapping in the bulk for bipolar transistors," *Noise Phys. Syst.* $1/f$ *Noise*, pp. 405–407, 1985.

[20] S. Mohammadi and D. Pavlidis, "A nonfundamental theory of low-frequency noise in semiconductor devices," *IEEE Trans. Electron Devices*, vol. 47, pp. 2009–2017, Nov. 2000.

[21] X. Zhang, A. Van der Ziel, K. Duh, and H. Morkoc, "Burst and low-frequency generation and recombination noise in double-heterojunction bipolar transistors," *IEEE Electron Device Lett*, vol. EDL-5, pp. 277–279, July 1984.

[22] T. G. M. Kleinpenning, "Low-frequency noise in modern bipolar transistors: Impact of intrinsic trnsistor and parasitic series resistances," *IEEE Trans. Electron Devices*, vol. 41, pp. 1981–1991, Nov. 1994.

[23] S. Tanaka, H. Shimawaki, K. Kasahara, and K. Honjo, "Characterization of current induced degradation in Be-doped HBTs based in GaAs and InP," *IEEE Trans. Electron Devices*, vol. 40, pp. 1194–1201, July 1993.

[24] A. Penarier, F. Pascal, S. G-Jarrix, C. Delseny, M. Riet, and S. Blayac, "Low frequency noise of InP/InGaAs Heterojunction bipolar transistors," *Jpn. J. Appl. Phys.*, vol. 40, pp. 525–529, Feb. 2001.

[25] H. Casey, Jr. and E. Buehler, "Evidence for low surface recombination velocity on n-type InP," *Appl. Phys. Lett.*, vol. 30, no. 5, pp. 247–249, Mar. 1977.

[26] J. M. Moison, J. M. Van Rompay, and M. Bensoussan, "Influence of the near-band-edge surface on the luminescence efficiency of InP," *Appl. Phys. Lett.*, May 19, 1986.

[27] S. Bothra, S. Tyagi, S. K. Ghandhi, and J. M. Borrego, "Surface recombination velocity and lifetime in InP," *Solid-State Electron.*, vol. 34, no. 1, pp. 47–50, Jan. 1991.

[28] A. Van der Ziel, "Formulation of surface $1/f$ noise process in bipolar junction transistors and in p-n diodes in Hooge-type form," *Solid-State Electron.*, vol. 32, no. 1, pp. 91–93, Jan. 1989.

[29] S. Hsu, D. Pavlidis, and D. Sawdai, "Low-frequency noise characteristics of p-n-p InAlAs/InGaAs HBTs," *IEEE Electron Device Lett.*, vol. 23, pp. 688–690, Dec. 2002.

Shawn S. H. Hsu was born in Tainan, Taiwan, R.O.C. He received the B.S. degree from the Electrical Engineering Department, National Tsing Hua University (NTHU), Taiwan, in 1992 and the M.S. and Ph.D. degrees from the University of Michigan, Ann Arbor, in 1997 and 2003, respectively.

From 1992 to 1994, he was a Lieutenant in the Taiwanese Army. From 1994 to 1995, he was a Research Assistant at National Chiao-Tung University, Taiwan. He is currently an Assistant Professor in the Electrical Engineering Department, NTHU, Hsinchu, Taiwan. His current research interests include development of analytical and empirical large-signal and noise equivalent circuit models of III–V/Si based devices for RFIC/MMIC design applications, the implementation and development of various measurement techniques to extract parameters for equivalent circuit models, and the design of MMICs and RFICs using III–V/Si based devices for low-noise, high-linearity, and high-efficiency system-on-chip (SOC) applications.

Dimitris Pavlidis (S'73–M'76–SM'83–F'93) received the B.Sc. degree in physics from the University of Patras, Patras, Greece, in 1972 and the Ph.D. degree in applied science/electronic engineering from the University of Newcastle, Newcastle-upon-Tyne, U.K., in 1976.

He has been Professor of electrical engineering and computer science at the University of Michigan, Ann Arbor, since 1986. He was an Invited Guest of the Institute of Semiconductor Electronics, Technical University of Aachen, Aachen, Germany, in 1974. He worked as Postdoctoral Fellow at Newcastle, from 1976 to 1978, engaged in work on microwave semiconductor devices and circuits. In 1978, he joined the High Frequency Institute, Technical University of Darmstadt, Germany, as a Lecturer working on III–V devices and establishing a new semiconductor facility. In 1980, he worked at the Central Electronic Engineering Research Institute, Pilani, India, as UNESCO consultant. From 1980 to 1985, he was an Engineer and a Manager of the GaAs Monolithic Microwave Integrated Circuits (MMIC) Department, Thomson-CSF, Corbeville, France. In this capacity, he was responsible for projects on various monolithic circuits, their technology and process evaluation. He was a Visiting Scientist of the Centre National d'Études des Télécommunications (CNET)/France Telecom, Bagneux, France, in 1993, and a Visiting Professor at the University of Hokkaido, Sapporo, Japan, in 1992, Meijo University, Nagoya, Japan, in 2000, and the University of Western Australia, Perth, Australia, in 2000. Since 1986, he has been involved in research on heterostructure devices and materials at the University of Michigan. This includes the design, fabrication and characterization of GaAs, InP-based HEMTs and HBTs, diodes for switching and mixing, GaN-based HFETs and two-terminal devices. His research also covers microwave/millimeter-wave monolithic heterostructure integrated circuits built with such devices. His materials research covers InP and III–V Nitride based heterostructures using metalorganic chemical vapor deposition (MOCVD) and their device application. His work in the above areas has been reported in numerous papers and reports and he holds six patents.

Dr. Pavlidis received the European Microwave Prize for his work in InP based monolithic integrated HEMT amplifiers, in 1990, the decoration of "Palmes Académiques" in the order of Chevalier by the French Ministry of Education for his work in education, in 1991, the Japan Society of Promotion of Science Fellowship for Senior Scientists/Professors from the Japanese Government, in 1992 and 1999, the Humbolt Research Award for Distinguished Senior U.S. Scientists, in 1992, the University of Michigan 1994 Electrical Engineering and Computer Science Award, and the 1996 College of Engineering Research Excellence Award.